# Using tip enhanced femtosecond lasers to create graphite nanostructures on diamond

**Contact** *s.m.bennington@rl.ac.uk*

**S.M. Bennington**
*STFC*
*Rutherford Appleton Laboratory, Chilton,*
*Didcot, Oxfordshire, OX11 0QX*

**R.I. Bewley**
*STFC*
*Rutherford Appleton Laboratory, Chilton,*
*Didcot, Oxfordshire, OX11 0QX*

**T.E. Weller**
*STFC*
*Rutherford Appleton Laboratory, Chilton,*
*Didcot, Oxfordshire, OX11 0QX*

**R.B Jackmann**
*London Centre for Nanotechnology*
*University College London, 17-19, Gordon Street, London,*
*WC1H 0AH*

## Introduction

Graphene has become one of the most dynamic areas of condensed matter physics due to an unusual conflation of interesting fundamental physics and the very real possibility of important technological applications. Not only is it an excellent condensed-matter analogue for two-dimensional quantum electrodynamics[1, 2], but it is also a zero band gap semiconductor with room temperature ballistic conduction and electron mobilities at least two orders of magnitude greater than in silicon.

Theoretical predictions of the transport properties of nanoscale graphene and graphite are particularly intriguing. Thin ribbons with largely zig-zag edges are predicted to be metallic and order magnetically, they are reported to be magnetic-resistive and even half metallic[3, 4] and by mixing in edge-states it is possible to open up the band-gap necessary to create electronic devices. To do this it is necessary to be able to control orientation of the ribbon with respect to the crystal structure.

Although much of the current interest is focused on graphene it now appears that some of its properties, such as presence of Dirac Fermions[5, 6] and ballistic conduction[7], are also present in graphite [8]. But research and technological application is hampered by a lack of sample. Although it is possible to produce high quality crystals of graphene of up to 100 µm through mechanical cleavage these methods are difficult to scale up and many groups are looking for alternatives. Our aim was to see if it was possible to grow thin layers of graphite through femtosecond laser irradiation of an atomically flat diamond (111) surface. Although we have demonstrated this and made progress in understanding the mechanisms of the diamond – graphite transformation the control of the thickness and lateral dimension has proved difficult. The thickness is controlled by multi-photon absorption and has a non-linear dependency with both wavelength and laser power and the lateral dimension is limited by the optical diffraction limit.

The aim of this research was to use tip enhancement to focus and amplify light intensity under the tip of a conducting atomic force microscope so that we can create structures on the surface of diamond smaller than the wavelength of laser.

To do this we made an application to use the femtosecond laser (UFL2) from the loan pool to build a prototype of a tip enhanced femtosecond laser and use it to create graphite nanostructures for transport measurements.

## Femtosecond irradiation of diamond

Heating the diamond (111) surface to temperatures of 2000K will transform it to graphite. This can be done in a furnace or with a laser with a pulse width of a nanosecond or more. However when the pulse length is reduced to the order of a hundred femtoseconds then there is no possibility for the electron-hole plasma reaching equilibrium with the lattice on the timescale of the laser pulse and recent theory and experiment indicate that the transformation is athermal and driven by the plasma itself[9, 10]. Our initial non-tip enhanced experiments appear to confirm this; showing the formation of small blisters of graphite which, are crystallographically aligned with the underlying diamond lattice. This means it should be possible to create nanostructures with controlled amounts of zig-zag and arm-chair edge-states and hence control the band-gap of a nano-graphitic ribbon.

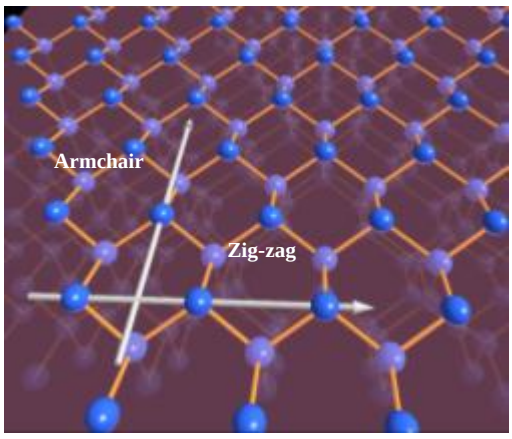


Figure 1: The (111) surface of diamond showing the puckered graphite like arrangement of the atoms. The two arrows show the armchair edge direction $(2\bar{1}\bar{1})$ or the zig-zag edge $(0\bar{1}1)$.

In our previous experiments using the CLF lasers we were able to irradiate an atomically flat diamond (111) surface with a 120fs laser pulse with wavelengths between 200 and 800nm. Diamond has an indirect band-gap of 5.4eV, but fitting of the transmission as a function of power shows that it is the direct band gap of 7.3eV that controls the production of electron-hole pairs[11]. As a consequence at all the wavelengths we are using the absorption processes are multi-photon and have a non-linear dependency with laser power. At 200 and 266nm we are firmly in the two-photon absorption region and we find that at above the graphitization threshold of 0.1 - 0.6 J/cm$^2$ we get a layer of

graphite with a thickness that scales with the absorption depth but with a relatively small crystallite size. But at 800nm we get well defined graphitic triangular crystals that are aligned with respect to the underlying diamond lattice and a have a crystallite size in excess of 80nm (Figure 2). These grow from relatively sparse nucleation sites, implying that there are defects in the diamond that have levels in the band gap to act as generators of electron-hole pairs.

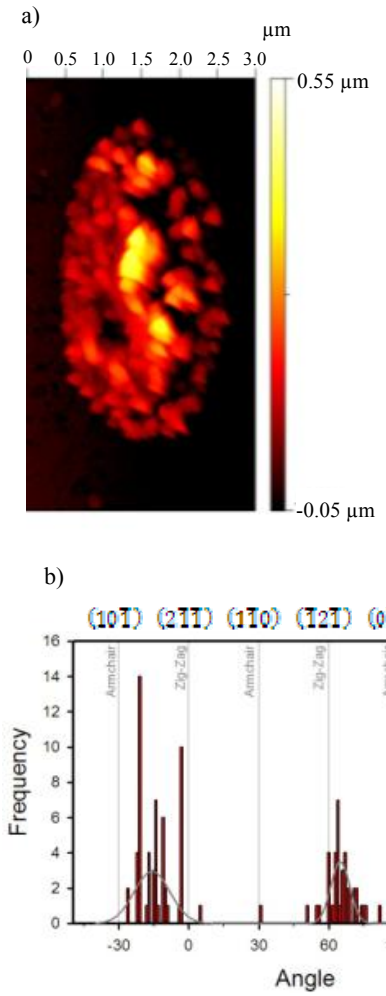


Figure 2: a) An Atomic Force Microscope height image showing triangular graphite crystals ~ 200nm across on the (111) surface of diamond. The spot was created with an 800nm 120fs laser pulse with an integrated energy of 3µJ. b) A plot of the distribution of surfaces in the edges of the triangles. The centres of the distributions are at -15 ± 2, 65 ± 1 and 119.8 ± 0.7 degrees and so the triangles are not equilateral but are clearly closer to zig-zag than armchair. The orientation of the triangles is consistent across the whole spot and between spots implying that they are related to the underlying crystal.

## Tip Enhancement

A metal tip brought close to a surface can create several orders of magnitude enhancement of the electric field through a combination of electrostatics and surface plasmon excitations that resonate with laser frequency. There have been rapid developments in techniques that use this tip enhancement for spectroscopy (Tip Enhanced Raman Spectroscopy, TERS) and optical microscopy (Scanning near-field Optical Microscopy, SNOM or aperture less SNOM, ASNOM)[12]. And there have been a few attempts to use it to modify surfaces by ablating metals or glass to create pits and lines and there have been measurements to modify the conductivity of hydrogen passivated silicon surfaces[13-18]. Although this idea has been in the literature for around 10 years it is only in the last 2 years that the first attempts have been made with femtosecond lasers.

This is clearly important for materials where the transformation processes is driven by high order multi-photon processes.

So far no-one has reported a method to transform a material from an insulator into a conductor or semiconductor. If we are able to do this on diamond or silicon carbide we would be able to write graphitic nano-electronic devices directly onto a surface with dimensions equal to those possible using state-of-the-art lithographic techniques in the electronics industry

### The experimental set-up

We focused the light from the UFL2 laser onto test surface and the tip of silicon tip the AFM. By using a highly attenuated beam it was possible to view the laser spot using the camera and optics of the AFM.

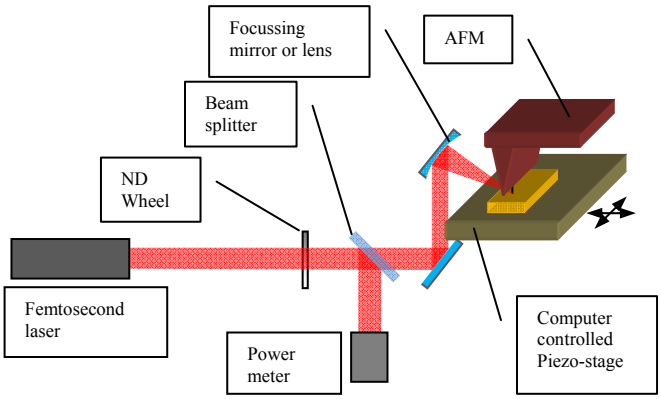


Figure 3: A schematic of the laser set-up that we envisage for the prototype.

All the initial set-up was done using a silicon wafer as the substrate. When the tip was advanced to the surface of the silicon the enhancement of the laser was immediately obvious as the tip glows brightly. We then set AFM to track a given path at a given speed along the surface in contact mode, whilst the laser was pulsed at up to 1000 pulses using 800nm wavelength and pulse with of 120fs.

### Results and discussion

During this set-up phase we found it possible to make sub-diffraction limit structures on the silicon with relative ease (figure 4). Switching to gold coated tips created an enhancement of between x10 – x100 tip enhancement because of the much more favorable Plasmon frequencies.

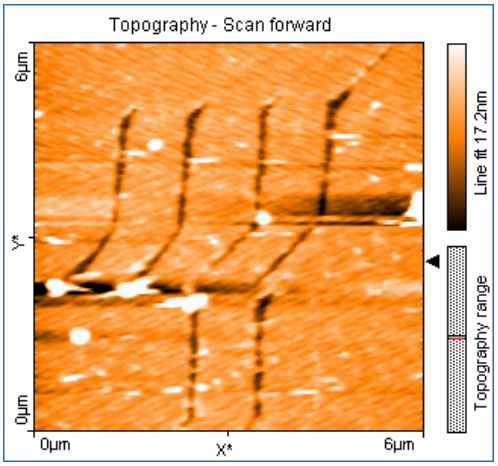


Figure 4: An AFM scan of structures written onto a silicon surface, using 800nm laser with a pulse with of 120fs running at 1000Hz. This is using a gold tipped AFM moving at speeds ranging 4 µm/s to 256 µm/s. The structures are trenches are approximately 100nm across.

However, we were not able to replicated this work on the diamond. This is probably partly due to the fact that the enhancement that you can achieve on a non-conducting surface is considerable smaller than for a conducting surface. We were hoping to able to excite electrons over the band gap to promote conductivity, but at 800nm we are relying on very high order multi-phonon processes. We were hoping to be able to use shorter wavelength laser light, but this proved impossible in the timescales available.

## Conclusions

Although we were able achieve tip enhanced structural changes on a conducting surface were not able to do this on the non-conducting diamond surface. It may still be possible to do this at shorter wavelengths.


## Acknowledgements

Proof of concept award from STFC Innovations and the supply of the atomically flat diamonds from Element 6.


## References


1. Novoselov, K.S., et al., *Two-dimensional gas of massless dirac fermions in graphene.* Nature, 2005. **438**: p. 197.
2. Zhang, Y., et al., *Experimental observation of the quantum hall effect and berry's phase in graphene.* Nature, 2005. **438**: p. 201.
3. Pisani, L., et al., *Electronic structure and magnetic properties of graphitic ribbons.* Physical Review B (Condensed Matter and Materials Physics), 2007. **75**.
4. Son, Y.W., M.L. Cohen, and S.G. Louie, *Half-metallic graphene nanoribbons.* Nature, 2006. **444**.
5. Luk'yanchuk, I.A. and Y. Kopeleich, *Phase analysis of quantum oscillations in graphite.* Physical Review Letters, 2004. **93**.
6. Zhou, S.Y., et al., *First direct observation of Dirac fermions in graphite.* Nat Phys, 2006. **2**(9): p. 595-599.
7. Gonzalez, J.C., et al., *Sample-size effects in the magnetoresistance of graphite.* Physical Review Letters, 2007. **99**.
8. Kopelevich, Y. and P. Esquinazi, *Graphene physics in graphite.* Advanced Materials, 2007. **19**: p. 4559-4563.
9. De Vita, A., et al., *A microscopic model for surface-induced diamond-to-graphite transitions.* Nature, 1996. **379**(6565): p. 523-526.
10. Kononenko, V.V., et al., *Effect of the pulse duration on graphitisation of diamond during laser ablation.* Quantum electronics, 2005. **35**(3): p. 252-256.
11. Preuss, S. and M. Stuke, *Subpicosecond ultraviolet laser ablation of diamond: Nonlinear properties at 248 nm and time-resolved characterization of ablation dynamics.* 1995, AIP. p. 338-340.
12. Gomez, L., et al., *Apertureless scanning near-field optical microscopy: a comparison between homodyne and heterodyne approaches.* Journal of the Optical Society of America, B, 2006. **23**(5): p. 823.
13. Nedyalkov, N.N., T. Miyanishi, and M. Obara, *Enhanced near field mediated nanohole fabrication on silicon substrate by femtosecond laser pulse.* Applied Surface Science, 2007. **254**: p. 6558-6562.
14. Li, K.J., Z.Y. Yang, and Y.F. Lu, *Fabrication of nanostructures with high electrical conductivity on silicon surfaces using a laser-assisted scanning tunneling microscope.* Journal of Applied Physics, 2007. **103**: p. 054307.
15. Chimmalgi, A., C.P. Grigoropoulos, and K. Komvopoulos, *Surface nanostructuring by nano/-femotosecond laser-assisted scanning force microscopy.* Journal of Applied Physics, 2005. **97**: p. 104319.
16. Huang, S.M., et al., *Pulsed laser-assisted surface structuring with optical near-field enhanced effects.* Journal of Applied Physics, 2002. **92**: p. 2495.
17. Mai, Z.H., et al., *Nano-modification on hydrogen-passivated Si surface by a laser-assisted scanning tunneling microscope operating in air.* Applied Surface Science, 2000. **154-155**: p. 360-364.
18. Dickmann, K., J. Jersch, and F. Demming, *Focusing of laser radiation in the near-field of a tip (FOLANT) for applications in nanostructuring.* Surface and Interface Analysis, 1997. **25**: p. 500-504.

# Nonlinear spectroscopy of doped glass and crystal for applications in distributed fibre sensing

**Contact** *i.s.ruddock@strath.ac.uk*

**I. S. Ruddock, C. J. Dalzell and T. P. J. Han**

*Nonlinear Spectroscopy and Sensing, Department of Physics*
*University of Strathclyde, SUPA, Glasgow G4 0NG, UK*

## Introduction

Fluorescence based sensing uses media doped with rare earth or transition metal ions in which the spectrum of the emitted fluorescence or the excited state decay time ($\tau$) depends on the external environment [1,2]. The strong temperature dependence of $\tau$ has enabled laboratory resolutions of <1°C to be demonstrated [3]. Its weak strain dependence can also be exploited in conjunction with the strain independence of the intensity ratio of thermally linked spectral lines to yield strain sensitivities of ~250 microstrain (με) [4]. In practice though, for the purposes of temperature sensing, the temperature to strain cross-sensitivity for most dopants is sufficiently small that even the application of a breaking strain only produces a temperature uncertainty of a few degrees Celsius. Existing fluorescence based sensors employ single-photon excitation and are thus point sensors in which a small sample of active material is attached to the end of a conventional optical fibre. The optical fibre plays no role other than to transmit the excitation light to the sample and to return the resulting fluorescence to a remote detector. Quasi-distributed sensing of discrete points using single-photon excited fluorescence (SPF) is only achievable by a network of such sensors. Currently, continuously distributed fibre sensing is achievable by optical time domain reflectometry of spontaneous and stimulated scattering, but these sensors frequently have limited temporal and spatial resolutions.

## Distributed optical fibre sensing based on two-photon excited fluorescence

The authors have previously shown [5-7] that two-photon excited fluorescence (TPF) may be exploited to achieve true distributed sensing. TPF is generated in an ionic medium by the simultaneous absorption of pairs of photons without the involvement of a real intermediate energy level. The sum of the photon energies in each pair matches the energy gap from the ground state to the higher energy level from which the ions relax with the eventual emission of fluorescence photons. With the TPF intensity being effectively proportional to the square of the total local photon flux, an enhanced fluorescence signal is produced where two laser pulses overlap. If the two pulses are counter-propagating in a doped optical fibre, their meeting point can be scanned along the length of the fibre by introducing a variable time delay between them. The resulting fluorescence flash from the overlap, usually in the visible or near infrared, is then transmitted along the fibre and detected and analysed at one end, Figure 1. With the length of the sensed position depending only on the pulse duration, there is the potential for high spatial resolution, while the total length of a fibre designed for two-photon absorption is intentionally transparent at the single-photon wavelength and is not normally limited by attenuation. Distributed TPF based sensing is equally applicable to mono- and multi-mode doped fibres allowing the technique to be extended to single crystal fibres such as sapphire with core diameters of 100s μm. Although modal dispersion of the excitation pulses will now reduce the spatial resolution, this will be more than compensated for in specific applications by their tolerance to much higher temperatures (~1500 °C) than glass fibres. Thus a TPF based sensor is expected to simultaneously possess high temporal (seconds), spatial (down to mm) and temperature (~1 °C) resolutions.

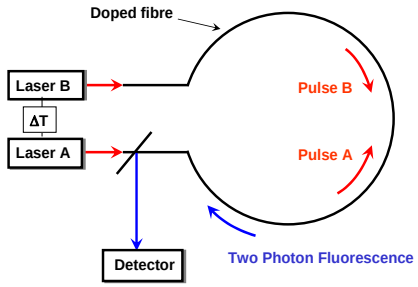


**Figure 1. Schematic diagram of a distributed sensor based on time-correlated TPF in a doped optical fibre. Counter-propagating pulses (A) and (B) meet at a location depending on their relative time delay, ΔT. The TPF generated at their overlap is guided along the fibre and detected.**

## Nonlinear spectroscopy

The aim of this work was to obtain the two-photon absorption spectrum for glass and crystal doped with various lanthanide and transition metal ions. Without such information, the feasibility of a distributed fibre sensor based on TPF cannot be assessed. The existing spectroscopic literature for these materials is mainly concerned with single-photon excitation linked to applications as laser media or fluorescence point sensors. Even for the latter, the published temperature and strain characteristics of the fluorescence lifetimes and spectra are generally not relevant to the approach described here as they have only been studied for the near-IR emission lines that arise from single-photon excitation and not visible TPF.

## Measurement of the two-photon absorption cross-section

Direct measurement of the two-photon absorption cross-section ($\delta$) is challenging because of the small absorption which has to be detected as well as knowing the ion concentration ($N_1$). To circumvent these difficulties, the TPF yield can be compared, under identical conditions, with that for SPF allowing $\delta$ to be deduced in terms of $\sigma$, the single-photon absorption cross-section. Although the unknown $N_1$ can now be eliminated, measurement of the fluorescence signals is non-trivial due to their vastly different magnitudes.

It is relatively straightforward to show for sample thicknesses ≤ 0.1 of an absorption length ($1/\sigma N_1$), that under excitation by nanosecond Gaussian pulses from a Q-switched laser,

$$\delta = \frac{1}{2}\sqrt{\frac{\pi}{2\ln 2}}\frac{A''t''_p hc}{\lambda''}\left(\frac{E'}{E''^2}\right)\left(\frac{P''(t)}{P'(t)}\right)\sigma \qquad (1)$$

where $P'(t)$ and $P''(t)$ are the SPF and TPF powers respectively, $E'$ and $E''$ are the energies of the SPF and TPF excitation pulses respectively, $\lambda''$ and $t''_p$ are the wavelength and FWHM duration of the TPF excitation pulses, and $A''$ is the area of the TPF excitation pulses in the sample. The quantum efficiencies for the two excitation schemes cancel when the same transition is involved in both cases, but accurate knowledge of $E'$ and $E''$, $t''_p$

and $A''$ at $\lambda''$ is still required to evaluate (1).

### The two-photon absorption spectrum of ruby

The two-photon absorption spectrum of ruby ($Cr^{3+}$:sapphire) is described here as an example of the type of measurement made. It helps complete the quantitative investigation of this important crystal which has been at the forefront of optoelectronics for over half a century as well as being the first practical laser medium. Related experiments on doped glass are outlined in the accompanying report – "Distributed sensing by time-correlated two-photon excited fluorescence in rare earth doped optical fibres" by I S Ruddock et al.

Transition metal ions offer broad absorption bands in the visible region. Cr is the most studied and the 'R-line' emission of ruby has been used in SPF based point sensors of pressure, strain and temperature by detecting the spectral shift of the fluorescent R-lines [1] and the change in the fluorescence decay time [2]. Sapphire fibres can be produced by laser heated miniature pedestal growth [8] and by extrusion [9].

The strong R-line fluorescence ($R_1$, 694.3 nm and $R_2$, 692.9 nm) is due to decay from the metastable $^2E$ state (the lowest lying component in the free ion's $^2G$ first excited state) back to the $^4A_2$ ground state (the lowest lying component in the free ion's $^4F$ ground state), Figure 2. The metastable $^2E$ state is split into $\bar{E}$ and $2\bar{A}$ states with an energy gap of ~29 $cm^{-1}$ by the nearly octahedral symmetry of the sapphire ($Al_2O_3$) host. The fluorescence decay time ($\tau$) decreases from ~3.5 ms at room temperature to ~45 μs at 650 °C and the R-lines shift slightly to longer wavelengths with increasing splitting, thus providing parameters for sensing purposes [10].

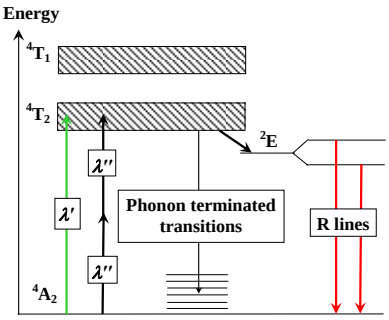


**Figure 2. Simplified energy level diagram for ruby showing single-photon ($\lambda'$) and two-photon ($\lambda''$) excitation.**

The measurements reported here were performed on a sample cut from a standard a-axis ruby rod. Excitation was provided by two Continuum pulsed systems: a Q-switched and frequency doubled Nd:YAG laser and the Laser Loan Pool's NSL3 optical parametric oscillator (OPO), both producing pulses with energies of 10s mJ and durations of ns. For light polarised along the ordinary and extraordinary axes of the crystal, the TPF and SPF signals were measured at 1.064 μm and 532 nm to determine discrete values of $\delta$ at 1.064 μm using equation (1) along with the appropriate values of $\sigma$ at 532 nm [11].

The wavelength dependence of $\delta$ over the 800–1200 nm range, i.e. the two-photon absorption spectrum, was obtained for the first time by recording the two-photon excitation spectra for the R-lines using the OPO's idler output and then converting them to absorption by normalising against (i) the square of the wavelength dependence of the OPO's photon flux, and (ii) the wavelength dependence of the fluorescence quantum efficiency [12], and finally scaling with the two values of $\delta$ already calculated for 1.064 μm, Figure 3.

The maximum values of $\delta$ observed were $5.9 \times 10^{-3}$ GM (1GM = $1 \times 10^{-50}$ $cm^4$.s.$ion^{-1}$.$photon^{-1}$) for e-polarisation and $4.6 \times 10^{-3}$ GM for o-polarisation at 840 nm. The overall uncertainty is ±40%, due primarily to the precision of the absolute quantities in equation (1). The random uncertainty in the underlying two-photon absorption spectrum is ±20%. In general, the two-photon and single-photon absorption spectra (inset in Figure 3) are similar. There are two broad bands of unequal strength corresponding to absorption from the ground state into $^4T_1$ and $^4T_2$ showing the same polarisation dependence. The longer wavelength peaks in $\lambda''$ at ~ 1100 nm agree well with those at ~ 2 × 550 nm in $\lambda'$. The shorter wavelength peaks at ~ 840 nm are offset by 30 nm from ~ 2 × 405 nm.

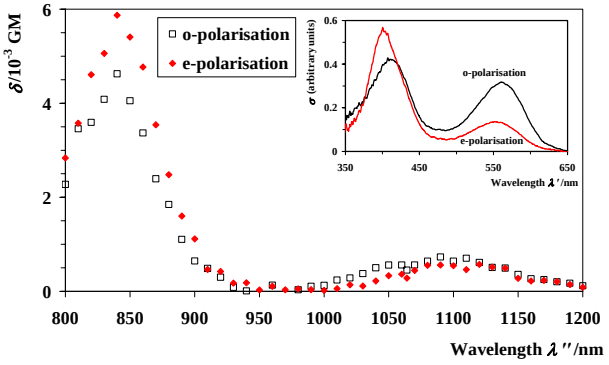


**Figure 3. The two-photon absorption spectrum of ruby for ordinary and extraordinary polarised light. The inset shows the normalised single-photon absorption spectrum.**

### Conclusions

Knowledge of $\delta$ for any fluorescent crystal or glass enables their use in a TPF based distributed optical fibre sensor to be assessed in the light of available lasers and other measurable and predictable parameters. Using the values reported here and the theory in [7], it can be shown that $>10^4$ fluorescence photons are detectable at one end of a ruby fibre of Cr density ~ $10^{17}$ $cm^{-3}$ (corresponding to a fluorescence self-absorption length of 10 m), diameter 100 μm, quantum efficiency ~0.9 and internal numerical aperture 0.38 (unclad sapphire) by pairs of counter-propagating 850 nm pulses of energy 1 μJ and duration 1 ns. In four-level media unlike ruby, self-absorption does not restrict the dopant density and the fibre is transparent for the fluorescence as well as the excitation pulses. Even with a decrease in the quantum efficiency at elevated temperatures, there is a sufficiently large fluorescence flux to enable $\tau$ to be measured rapidly and with precision.


### Acknowledgements

The use of the NSL3 OPO from the Laser Loan Pool is gratefully acknowledged by the authors. Craig Dalzell also acknowledges support by an Engineering and Physical Science Research Council postgraduate studentship.


### References


[1] R. A. Forman *et al., Science* 176, 284 (1972).
[2] R. R. Sholes *et al., Rev. Sci. Instr.* 51, 882 (1980).
[3] S. F. Collins *et al., J. Appl. Phys.* 84, 4649 (1998).
[4] S. A. Wade *et al., Rev. Sc. Instr.* 71, 2267 (2000).
[5] I. S. Ruddock and T.P.J. Han, *Sensors & their Applications XIII, J. Phys.: Conf. Series* 15, 83 (2005).
[6] I. S. Ruddock and T.P.J. Han, *Opt. Lett.* 31, 891 (2006).
[7] C. J. Dalzell, T. P. J. Han and I. S. Ruddock, *Appl. Phys.* B 93, 687 (2008).
[8] M.M. Fejer *et al., Rev. Sci. Instr.* 55, 1791 (1984).
[9] H.E. LaBelle, *J. Cryst. Growth* 50, 8 (1980).
[10] H. C. Seat and J. H. Sharpe, *IEEE Trans. Instr. and Meas.* 53, 140 (2004).
[11] D.C. Cronemeyer, *J. Opt. Soc. Am.* 56, 1703 (1966).
[12] T.H. Maiman *et al., Phys. Rev.* 123, 1151 (1961).

# Distributed sensing by time-correlated two-photon excited fluorescence in rare earth doped optical fibres

**Contact** *i.s.ruddock@strath.ac.uk*

**I. S. Ruddock, C. J. Dalzell and T. P. J. Han**

*Nonlinear Spectroscopy and Sensing, Department of Physics*
*University of Strathclyde, SUPA, Glasgow G4 0NG, UK*

**D. B. Hollis**

*School of Engineering*
*University of the West of Scotland, Paisley PA1 2BE, UK*

## Introduction

Continuously distributed fibre sensing is normally achieved by optical time domain reflectometry of spontaneous and stimulated scattering, but these sensors frequently have limited temporal and spatial resolutions. Alternatively, the environmental dependence of the fluorescence spectrum or the excited state decay time ($\tau$) for glass or crystal media doped with rare earth or transition metal ions can be exploited [1,2]. Additional detail on distributed sensing based on two-photon excited fluorescence (TPF) is contained in the accompanying report – "Nonlinear spectroscopy of doped glass and crystal for applications in distributed fibre sensing" by I. S. Ruddock et al., along with related experiments on the measurement of the two-photon absorption cross-section.

The basic approach of distributed sensing by fluorescence is that counter-propagating laser pulses in a doped fibre generate enhanced TPF at their overlap due to the absorption at this point being proportional to the square of the total local photon flux. The TPF is guided by the fibre to a detector at one end, while the overlap position can scanned along the fibre by means of a variable delay between the excitation pulses. Experiments and simulations show that a TPF based sensor is expected to simultaneously possess high temporal (seconds), spatial (down to mm) and temperature (~1 $^{o}$C) resolutions.

Despite the two-photon absorption cross-section ($\delta$) being of the order of 1 GM (= $1 \times 10^{-50}$ cm$^4$.s.ion$^{-1}$.photon$^{-1}$), sufficiently large TPF powers can be generated with relatively modest diode laser sources. With the spatial resolution depending only on the extent of the pulses' overlap, i.e. their second-order cross-correlation, even 'long' ns pulses still correspond to spatial resolutions of 10s cm. Surprisingly however, the use of such pulses does not affect the amount of TPF generated - the TPF produced at the overlap depends only on the energies of the excitation pulses and not their intensities or temporal profiles [3]. This is effectively due to a trade-off between the intensity of the stationary overlap region and the number of ions illuminated, in contrast to what would happen if TPF is generated by transient pulses away from the overlap. As TPF based sensing is equally applicable to mono- and multi-mode doped fibres, the technique can be extended to single crystal fibres with core diameters of 100s μm. Although modal dispersion of the excitation pulses will now reduce the spatial resolution, this will be more than compensated for in specific applications by their tolerance to much higher temperatures (~1500 $^{o}$C) than glass fibres.

## Two-photon excitation spectroscopy

The identification of potential TPF based sensing media was performed by exciting bulk samples of rare earth doped fluoride and silicate glass with the tuneable near-infrared idler and the visible signal outputs from the Laser Loan Pool's NSL3 optical parametric oscillator (OPO). Single- and two-photon excitation spectra were recorded by monitoring the fluorescence from various emission lines in each sample. Two-photon excitation spectra show the optimum wavelengths for excitation, but must be used in conjunction with appropriate single-photon excitation spectra to ensure that true TPF is being observed and not two-step fluorescence; in two-step fluorescence, a real intermediate energy level is excited by the first photon from which the second photon promotes the ion to the upper energy level where it relaxes with the eventual emission of a fluorescence photon. In the most general model of the sensor, the counter-propagating pulses can separately produce background TPF of the same wavelength as the TPF flash from their overlap. Detailed spectral information is necessary for choosing non-degenerate excitation wavelengths that only produce TPF at the overlap of the pulses and not individually. A fuller discussion of the choice of pulse wavelengths, energies and durations, and the impact of fibre length is given in reference [3]. Also, by comparing the fluorescence yield for single-photon excited fluorescence with that for TPF, $\delta$ can be determined [4].

Two-photon and two-step excited fluorescence was observed in praseodymium, samarium, europium, gadolinium, terbium, dysprosium, holmium and thulium [5], Figure 1. From this list, praseodymium was selected for detailed investigation in single-mode fibre geometry on account of its convenient excitation and TPF wavelengths and its potentially negligible fluorescence self-absorption due to the transitions of interest near 600 nm terminating above the ground state.

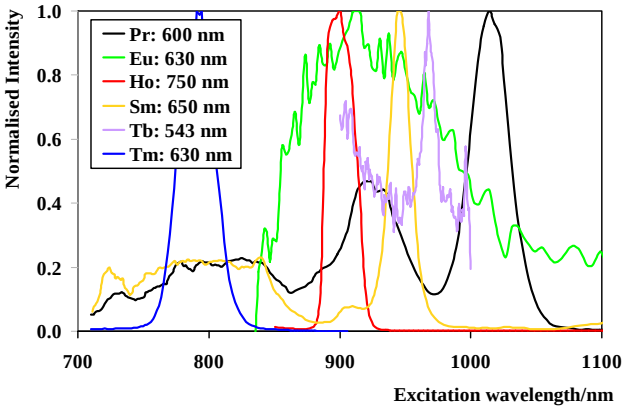


**Figure 1. Two-photon and two-step excited excitation spectra for a range of rare earth doped glasses of different composition. The corresponding emission wavelengths are indicated in the legend. For praseodymium (black line), note the TPF excitation peak at ~930 nm and the adjacent two-step excited fluorescence peak at ~1014 nm.**

### TPF in praseodymium doped fibre

Figure 2 shows the TPF spectrum at ~600 nm from 10 m of praseodymium doped single-mode fibre. The OPO's idler at 930 nm excited the ions in the vicinity of the $^3P$ manifold centred on ~2100 $cm^{-1}$ above the $^3H_4$ ground state. The principal emission contains lines at ~595 nm, ~620 nm and ~635 nm. These are a superposition of transitions from $^3P_o$ and the lower lying $^1D_2$, which is populated radiationlessly from the former.

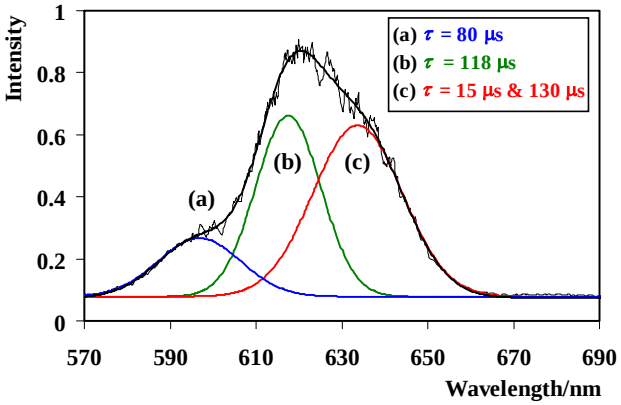


**Figure 2. The TPF spectrum for praseodymium doped silica fibre showing the composite emission line at ~600 nm, the de-convolved components and their respective room temperature decay times, $\tau$.**

By comparing the effects of self-absorption in short and long lengths of fibre, the tentative identification of the components is that the 595 nm line corresponds to $^1D_2 \rightarrow {}^3H_4$ but those at 620 nm and 635 nm are $^3P_o \rightarrow {}^3H_6$ and $^3P_o \rightarrow {}^3F_2$ respectively, Figure 3. As neither of these two longer wavelength TPF transitions terminate on the ion's $^3H_4$ ground state, they are suitable for distributed sensing over long paths.

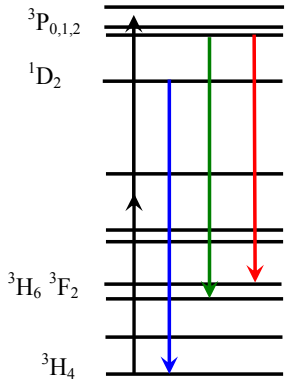


**Figure 3. The energy level structure of praseodymium showing the fluorescence transitions following two-photon excitation at 930 nm.**

The room temperature values of the fluorescence decay times for the three transitions are listed in the inset in Figure 2. The room temperature decay curve for the 620 nm emission is shown in Figure 4 along with its temperature dependence in the inset. With only 5000 data points, a 5% precision in the fitted lifetime is obtained even under two-photon excitation. This indicates that good temperature and temporal resolutions and short acquisition times will be achievable when a high repetition rate source (~1000 Hz) is employed in a prototype sensor instead of the 10 Hz OPO used here. Preliminary measurements of the time development of the TPF produced by degenerate counter-propagating pulses at 930 nm suggest that enhanced fluorescence (the TPF flash) is indeed being generated at their overlap as predicted by the authors' theoretical model [6].

### Conclusions

The use of the Laser Loan Pool's NSL3 OPO for investigating the two-photon excited fluorescence spectroscopy of rare earth doped glass and optical fibre has been summarised. New transitions in the visible suitable for distributed optical fibre sensing have been identified. Matched single-photon and two-photon excitation spectra for the same transitions have been recorded for certain dopants and their forthcoming analysis will enable the two-photon absorption cross-sections to be determined for these specific ion-glass combinations for the first time.


### Acknowledgements

The loan of the NSL3 OPO is gratefully acknowledged by the authors. Craig Dalzell acknowledges support by an Engineering and Physical Science Research Council postgraduate studentship. The authors also thank OFS, Denmark for the supply of R31501-Pr fibre.


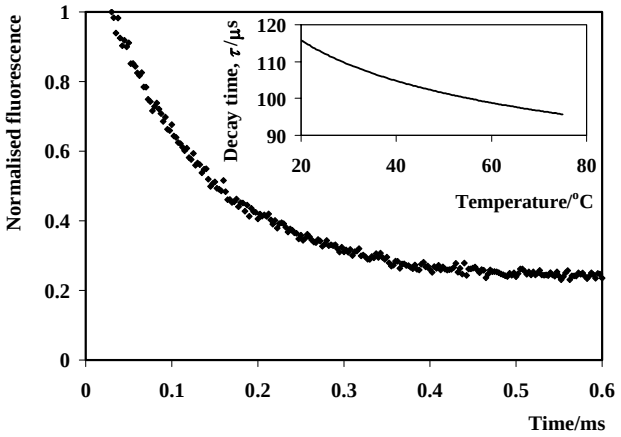


**Figure 4. The room temperature decay of the 620 nm fluorescence from praesodymium doped fibre; $\tau$ = 118 μs. The inset shows the temperature dependence of $\tau$.**

### References


[1] R. A. Forman, G. J. Piermarini, J. D. Barnett and S. Block, *Science* 176, 284 (1972).

[2] R. R. Sholes and J. G. Small, *Rev. Sci. Instr*. 51, 882 (1980).

[3] C. J. Dalzell, T. P. J. Han and I. S. Ruddock, *Appl. Phys.* B 93, 687 (2008).

[4] C. J. Dalzell, T. P. J. Han, I. S. Ruddock, submitted (2010).

[5] C. J. Dalzell, T. P. J. Han, I. S. Ruddock and D. B. Hollis, unpublished.

[6] I. S. Ruddock and T.P.J. Han, *Opt. Lett*. 31, 891 (2006).